



OPEN

Development and performance evaluation of a PTO-based power assist system to improve traction force for electric tractors

Ahn Da-Vin¹, Kyeongdae Kim¹, Seung-Je Cho¹, Kyujeong Choi¹, Ji-Tae Kim² & Wongun Kim¹✉

Electrification of agricultural machinery is crucial for meeting environmental regulations, with electric tractors being a prime example. However, insufficient power during high-load operations, such as plow tillage, limits the field applicability of conventional electric tractors. To address this, we propose and evaluate a Power Take-Off (PTO)-based power-assist system to supplement the traction power. Three powertrain configurations were modeled and compared: (i) a baseline dual-motor coupling powertrain (DMCP), (ii) a speed-coupling DMCP with power-assist system, and (iii) a mixed-coupling DMCP with power-assist system. The performance was evaluated under measured plow tillage conditions, focusing on traction force, travel speed, and energy consumption, with the latter assessed using an optimal control strategy derived via dynamic programming. Under a demanding 55 kW workload, only the assist-equipped configurations operated within the required power envelope. The speed-coupling configuration delivered the highest traction torque through torque amplification, despite a slightly reduced maximum speed. This configuration also lowered energy consumption by up to 2.40% compared to the baseline DMCP. These findings confirm the proposed PTO-based power-assist system is a practical solution for enhancing high-load operability and energy efficiency without major powertrain modifications. Future work will focus on hardware-in-the-loop validation of the proposed configuration.

Keywords Electric tractor, Dual motor coupling powertrain, Power assist system, Dynamic programming, Agricultural work

The electrification of agricultural machinery has emerged as a promising strategy to comply with environmental regulations and reduce carbon emissions from farming operations¹. Electric tractors have gained attention as representative eco-friendly solutions for the electrification of agricultural machinery. These tractors offer several advantages, including reduced exhaust emissions, minimal noise levels, and enhanced energy efficiency, thereby contributing significantly to sustainable farming².

Research on electric tractors can be divided into two areas: (1) studies focusing on the configuration of electric tractor powertrains, and (2) studies on control algorithms for electric tractors. Research on electric-tractor powertrain configurations is primarily categorized into two distinct strands. First, studies were conducted on single-motor structures that replace engines in conventional internal combustion tractors with electric motors³. Powertrain configurations employ two or more motors^{2,4–9}. Melo⁶ reported a dual-motor application on a 9 kW electric tractor featuring an in-wheel motor on each rear wheel to provide tractive drive. While suitable for traction-dominant tasks, this powertrain configuration does not account for hydraulic or PTO power demands, thereby limiting its applicability across typical farming operations. Research on control algorithms for electric tractors has primarily focused on strategies for enhancing energy efficiency^{10–13} and improving the performance of a given architecture^{14,15}. However, most of this research was conducted under the assumption that the specifications of the electric tractor system have already been determined. In conventional agricultural operations, a single tractor is used for various tasks including plowing, rotary tilling, and transportation¹⁴. This poses a significant challenge because conventional electric tractors may exhibit diminished operational efficiency or an inability to execute high-power-demanding tasks, such as plowing in heavy soil conditions,

¹Jeonbuk Technology Application Division (Specialized Machinery) Specialized Machinery and Robotics Group, Korea Institute of Industrial Technology, Gimje 54325, South Korea. ²Department of Convergence Biosystems Engineering, Chonnam National University, 77 Yongbong-ro, Buk-gu, Gwangju 61186, South Korea. ✉email: wjk@kitech.re.kr

owing to inadequate power output. Potential solutions to address this issue include the adoption of a multi-speed mechanical gearbox, modification of motor specifications, and an increase in the number of motors. However, the integration of a multi-speed mechanical gearbox not only increases the structural complexity and concomitantly reduces the energy efficiency¹⁶, but its modification is also challenging because any alteration is contingent upon a comprehensive overhaul of the powertrain configuration. To overcome these limitations, this study proposes a power-assist system designed to enhance propulsion capability while minimizing modifications to the existing powertrain configuration. Specifically, the proposed configuration supplements the baseline dual-motor coupling powertrain (DMCP) by incorporating an auxiliary motor via a power-take-off (PTO) shaft. The efficacy of this approach was evaluated through a comparative analysis of the baseline configuration.

The contributions of this study are summarized as follows (1) This study proposes a novel powertrain configuration, the DMCP with power assist system, which supplements a baseline DMCP by incorporating an auxiliary motor via a PTO shaft. (2) To facilitate comparative performance analysis, we developed simulation models and control algorithms for both the baseline and proposed configurations. (3) The effectiveness of the proposed system is validated through dynamic and economic performance analyses under identical plow tillage conditions.

The novelty of this study is threefold: (1) A hardware-based approach to enhance the tractive performance of electric tractors is proposed, which is compatible with various powertrain configurations. (2) Propose and comparatively evaluate two novel DMCP-based powertrain configurations, defined by the distinct relationships between motor torque and speed. (3) The proposed and baseline configurations were evaluated using an optimal control strategy, thereby eliminating performance biases attributable to the control strategies.

Methods

Power assist system description

A power-assist system is designed to provide supplementary tractive effort, particularly under demanding operating conditions where the native powertrain of the tractor is insufficient to meet the performance requirements. The power-assist system proposed in this study operates by supplying additional power to the powertrain from an assist motor coupled to a PTO shaft. The baseline of this study was a DMCP configuration. In this configuration, the two motors serve as power sources, and their combined output is transmitted to the powertrain¹⁷. Compared with a single-motor equivalent, this architecture enables operation at more efficient points under various load conditions, thereby enhancing the overall powertrain efficiency¹⁶. Figure 1 illustrates the proposed powertrain configuration, in which a power-assist system is integrated into a baseline DMCP. As shown, the system enables high-load operability by coupling an assist motor to an existing PTO shaft, thereby enhancing the capability of the tractor to perform demanding agricultural tasks.

Dual-motor coupling powertrain: speed-coupling type (DMCP: speed-coupling)

The dual-motor coupling powertrain configuration adopted in this study was of the speed coupling type, as illustrated in Fig. 2. This configuration comprised two motors (a main motor and an auxiliary motor), two clutches (C1 and C2), a brake (B1), input gears for each motor, a planetary gear set, a two-speed transmission, a PTO gear, and a final drive. In this speed-coupling configuration, the power from the main and auxiliary motors is combined with the planetary gear set and subsequently transmitted to a two-speed transmission. The planetary gearset features two input members (the ring and sun gears) and one output member (the carrier). The main motor is connected to the ring gear via its respective input gear, whereas the auxiliary motor drives the sun gear. The powers from both inputs were merged at the carrier and transmitted to the final drive. The operating modes of the speed-coupling configuration are distinguished by the power flow path, which is determined by the engagement of the clutches and brake. Accordingly, the modes were defined based on the number of active motors, selected transmission gear stage, and specific agricultural tasks, as detailed below.

1) Dual mode

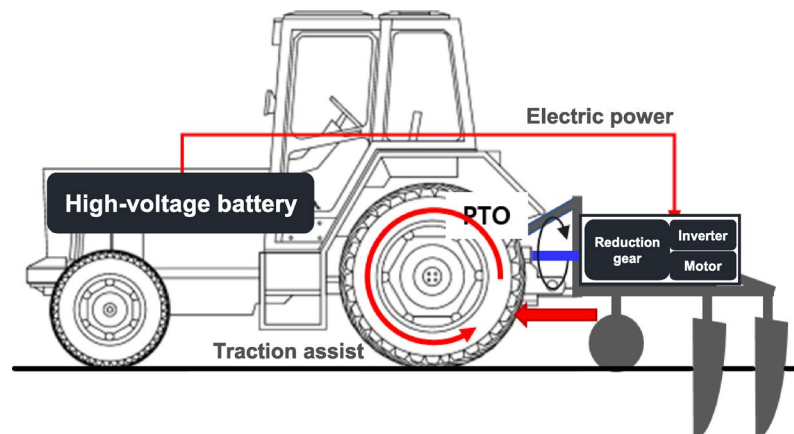


Fig. 1. Structure electric tractor with power assist system.

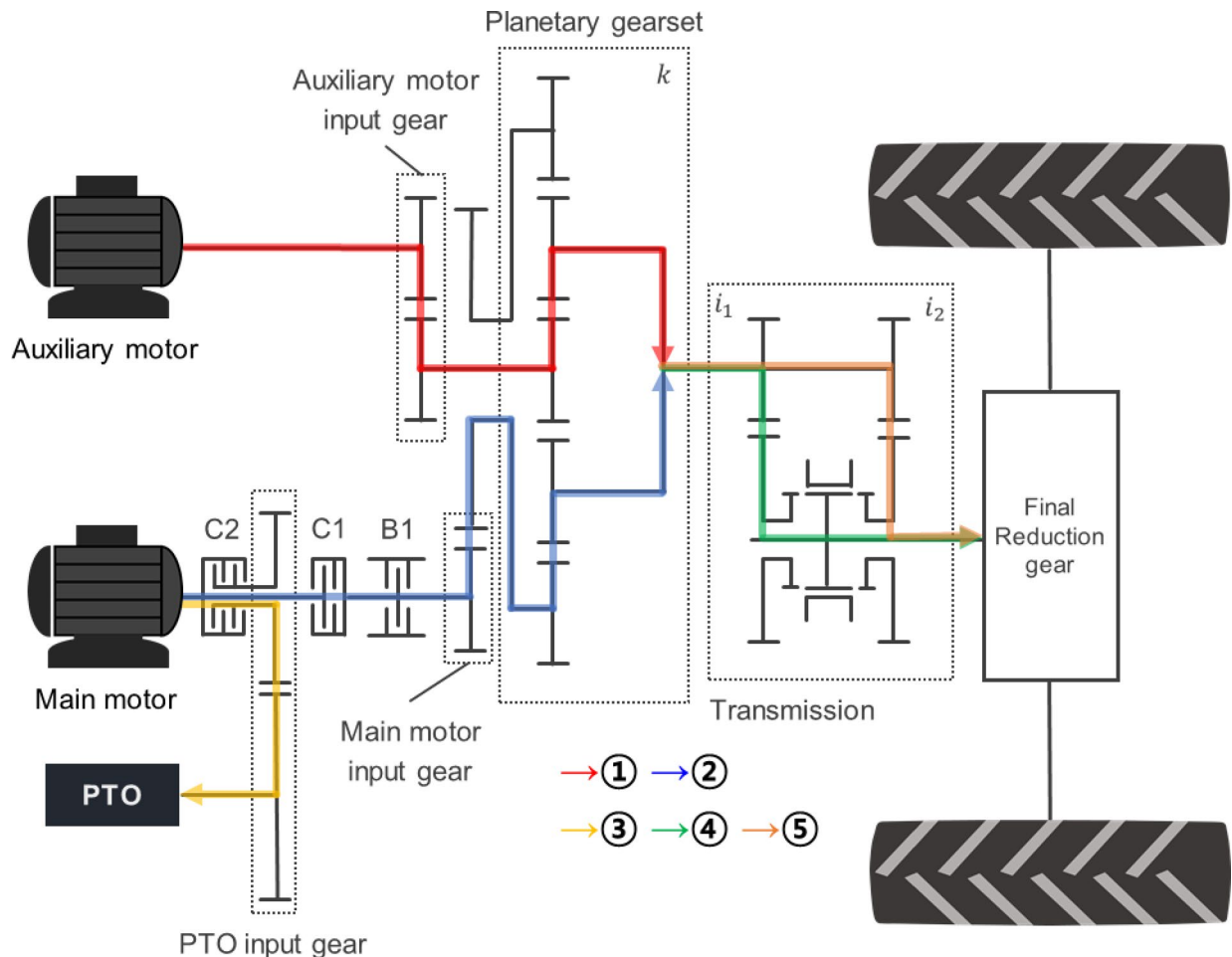


Fig. 2. Dual-motor coupling powertrain: speed-coupling type.

The dual-motor mode is employed for demanding tasks such as plow tillage or transport operations, which do not require PTO power. Gear selection is determined by the torque-speed requirements of the task; the first gear is selected for low-speed, high-torque conditions, whereas the second gear is used for high-speed, low-torque operations.

In both gear stages, the power from the main motor is transmitted to the planetary gear of the gearset, with clutch C1 engaged and clutches C2 and B1 disengaged. Simultaneously, the auxiliary motor transmitted torque to the sun gear. The combined output from the carrier was then routed through a two-speed transmission to the wheels. As illustrated in Fig. 2, power is transmitted along different paths depending on the gear stage. In the first gear, the power from the main motor is routed through Paths 2 and 4, whereas the auxiliary motor uses Paths 1 and 4. In the second gear, the power of the main motor follows Paths 2 and 5, and the power of the auxiliary motor is transmitted along Paths 1 and 5.

2) PTO mode

The PTO mode is employed for agricultural tasks that require PTO power, such as rotary tillage. In this mode, the main and auxiliary motors operate concurrently yet independently, with the transmission set to second gear. This independent operation allows the main motor to maintain the required PTO rotational speed, while the auxiliary motor controls the travel speed of the tractor. Power from the main motor is delivered to the PTO shaft, which requires clutch C1 to be disengaged, and clutches C2 and B1 to be engaged. Simultaneously, the auxiliary motor provided tractive power by transmitting torque to the wheels. As illustrated in Fig. 2, the corresponding power paths are line 3 for the main motor, and lines 1 and 5 for the auxiliary motor.

Table 1 summarizes the operating states of the powertrain components in each operating mode of the speed-coupled DMCP.

DMCP with power assist system: speed-coupling type

In a speed-coupling DMCP with a power-assist system, the assist motor is mechanically coupled to the PTO shaft and transmits power to the input gear of the main motor, as illustrated in Fig. 3. Consequently, the direct connection between the PTO input and assist gears mechanically couples the rotational speeds of the main and

Operating mode	Mainmotor	Auxiliary motor	Clutch		Brake	TransmissionRatio	
			C1	C2		1st gear	2nd gear
Dual mode 1	●	●	●	○	○	●	○
Dual mode 2	●	●	●	○	○	○	●
PTO mode	●	●	○	●	●	●	○

Table 1. Operating modes of the DMCP speed-coupling type. • indicates that the motor is on or the brake is engaged, ○ indicates that the motor is off or the brake is disengaged

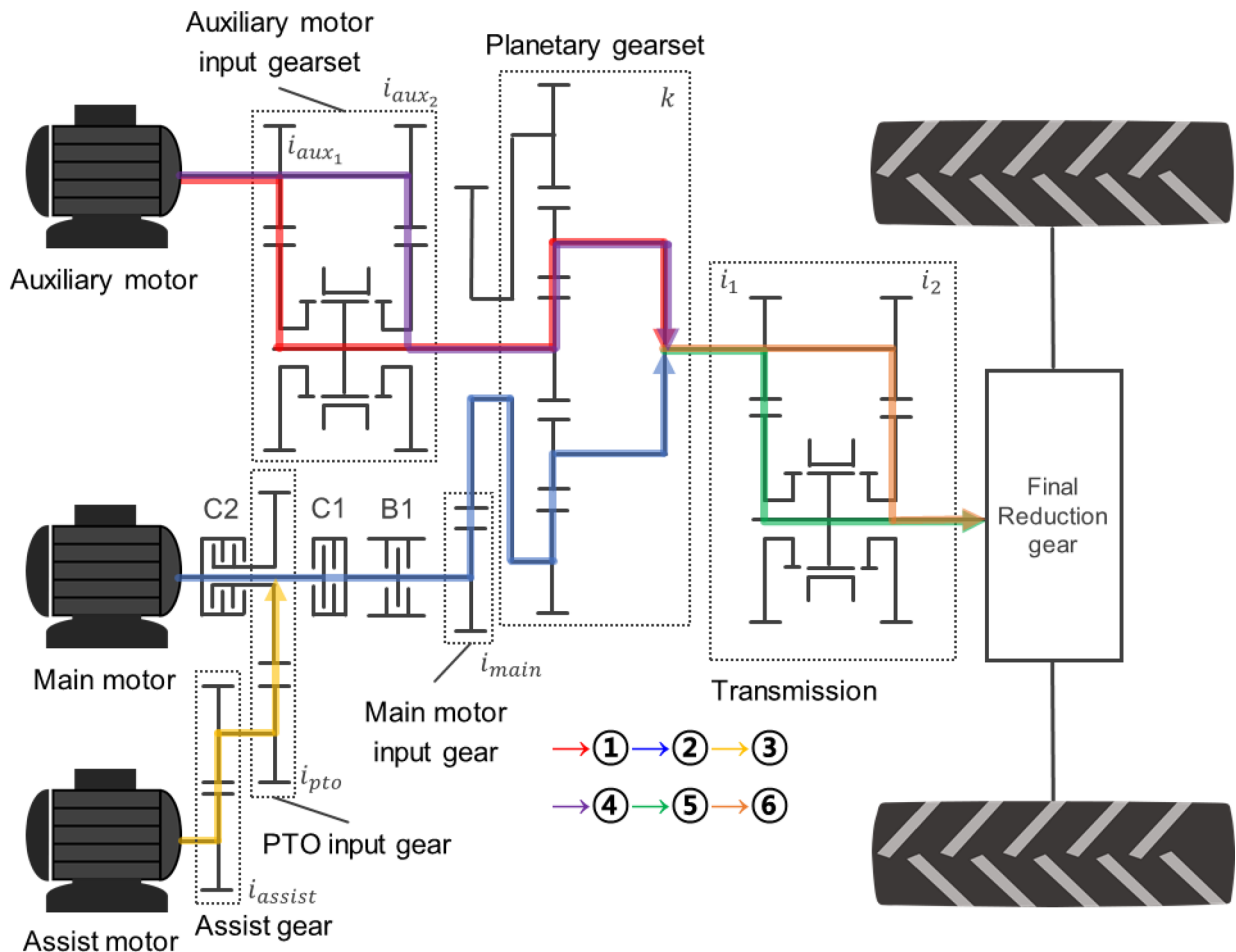


Fig. 3. DMCP with power assist system: speed-coupling type.

assist motors. In contrast, the auxiliary motor, which drives the sun gear, operates independently of the main and assist motors. The proposed powertrain configuration is a speed-coupling DMCP with a power-assist system, as shown in Fig. 3. This configuration consists of three electric motors (main, auxiliary, and assist), two clutches (C1 and C2), a brake (B1), input gears for each motor, a planetary gear set, a two-speed transmission, and a final drive.

In this configuration, the combined torque from the main and assist motors is transmitted to the ring gear, and the auxiliary motor provides torque to the sun gear. The total torque is then merged at the carrier and transmitted to drive the wheels. The operating modes are determined by the usage of the motor and the engagement state of the clutches and brake and are categorized as follows:

1) Dual mode

The dual-mode employs the main and auxiliary motors as power sources, operating similarly to the baseline DMCP. The transmission gear stage is selected based on the task's torque-speed requirements: the first gear is employed for low-speed, high-torque demands, such as plowing, while the second gear is used for high-speed, low-torque operations, such as transport. The power flows for both the gear stages are as follows: With clutch C1 engaged and C2 and B1 disengaged, the power from the main motor is transmitted to the ring gear of the

planetary gearset. Simultaneously, the auxiliary motor delivers torque to the sun gear through the auxiliary motor input gearset, which has a gear ratio i_{aux1} . The resulting torque on the carrier is then transmitted through a two-speed transmission to drive the wheels. The power flow paths for the main and auxiliary motors, illustrated in Fig. 3, change with the selected gear. In the first gear, the power follows paths 2 and 5 from the main motor and paths 1 and 5 from the auxiliary motor. In the second gear, these paths shift to 2 and 6 for the main motor, and 1 and 6 for the auxiliary motor.

2) Assist mode

The assist mode is the operating mode in which all three motors (main, auxiliary, and assist) are active. The transmission gear is selected based on the task requirements: the first gear is employed for low-speed, high-torque conditions, such as plowing, whereas the second gear is used for high-speed, low-torque operations, such as transport. In both gear stages, the combined torque from the main and assist motors is transmitted to the planetary gear of the gearset, which is achieved with engaged clutches C1 and C2 engaged and brake B1 disengaged. Simultaneously, the auxiliary motor delivers torque to the sun gear through the auxiliary motor input gearset, which has a gear ratio i_{aux2} . The resulting total torque is then output from the carrier and transmitted through the transmission system to drive the wheels. The power flow paths for each gear stage, as illustrated in Fig. 3, are as follows. In the first gear, the main motor used paths 2 and 5, the auxiliary motor used paths 4 and 5, and the assist motor followed paths 3, 2, and 5. In the second gear, the power from the main motor is transmitted along paths 2 and 6, and the auxiliary motor is transmitted along paths 4 and 6, and the assist motor is transmitted along paths 3, 2, and 6.

3) PTO mode

The PTO mode functions similarly to the baseline DMCP and is activated by disengaging the assist motor. In this mode, the main motor transmits power to the PTO shaft via the assist and input gears when clutch C1 is disengaged, and C2 and B1 are engaged. Simultaneously, the auxiliary motor delivered power to the drive wheels for traction. As illustrated in Fig. 3, the power from the main motor flows in the reverse direction of line 3, whereas the power from the auxiliary motor is routed along lines 1 and 5.

Table 2 summarizes the engagement states of each component for all operating modes.

DMCP power assist system: mixed-coupling type

In a mixed-coupling DMCP with a power-assist system, the assist motor is mechanically coupled to the PTO shaft and delivers torque to the carrier (the output shaft of the planetary gearset) via a dedicated power-assist gear, as illustrated in Fig. 4. This powertrain configuration consists of three motors (main, auxiliary, and assist), two clutches (C1 and C2), one brake (B1), the aforementioned power-assist gear, the main motor input gear, a planetary gear set, a two-speed transmission, and a final drive. In this configuration, the torques from the main and auxiliary motors are combined within the planetary gear set and transmitted to the carrier. When the assist motor is active, it supplies additional torque to the carrier, thereby increasing the total output torque transferred to the drive wheels. The operating modes are categorized based on the combination of active motors and the engagement states of the clutches and brakes, as detailed below.

1) Dual mode

The dual-mode operates identically to the corresponding mode of the baseline DMCP, employing only the main and auxiliary motors. The transmission gear stage is selected based on a specific agricultural task: the first gear is for low-speed, high-torque operations, such as plowing, whereas the second gear supports high-speed, low-torque conditions, such as transport. In both gear stages, the power from the main motor is transmitted to the ring gear of the planetary gearset, with clutch C1 engaged, and both C2 and B1 disengaged. Simultaneously, the auxiliary motor delivered torque to the sun gear. The combined torque is then output from the carrier and routed through the transmission to the drive wheels. As illustrated in Fig. 4, the power paths for the main and auxiliary motors are, respectively, lines 2 and 5, and lines 1 and 5 in the first gear. In the second gear, these paths shift to lines 2 and 6, and 1 and 6.

2) Assist mode

Operating mode	Mainmotor	Auxiliary motor	Assistmotor	Clutch		Brake	TransmissionRatio	
				C1	C2		1st gear	2nd gear
Dual mode 1	●	●	○	●	○	○	●	○
Dual mode 2	●	●	○	●	○	○	○	●
Assist mode 1	●	●	●	●	●	○	●	○
Assist mode 2	●	●	●	●	●	○	○	●
PTO mode	●	●	○	○	●	●	●	○

Table 2. Operating modes of the DMCP power assist system: speed-coupling type. ● indicates that the motor is on or the brake is engaged, ○ indicates that the motor is off or the brake is disengaged.

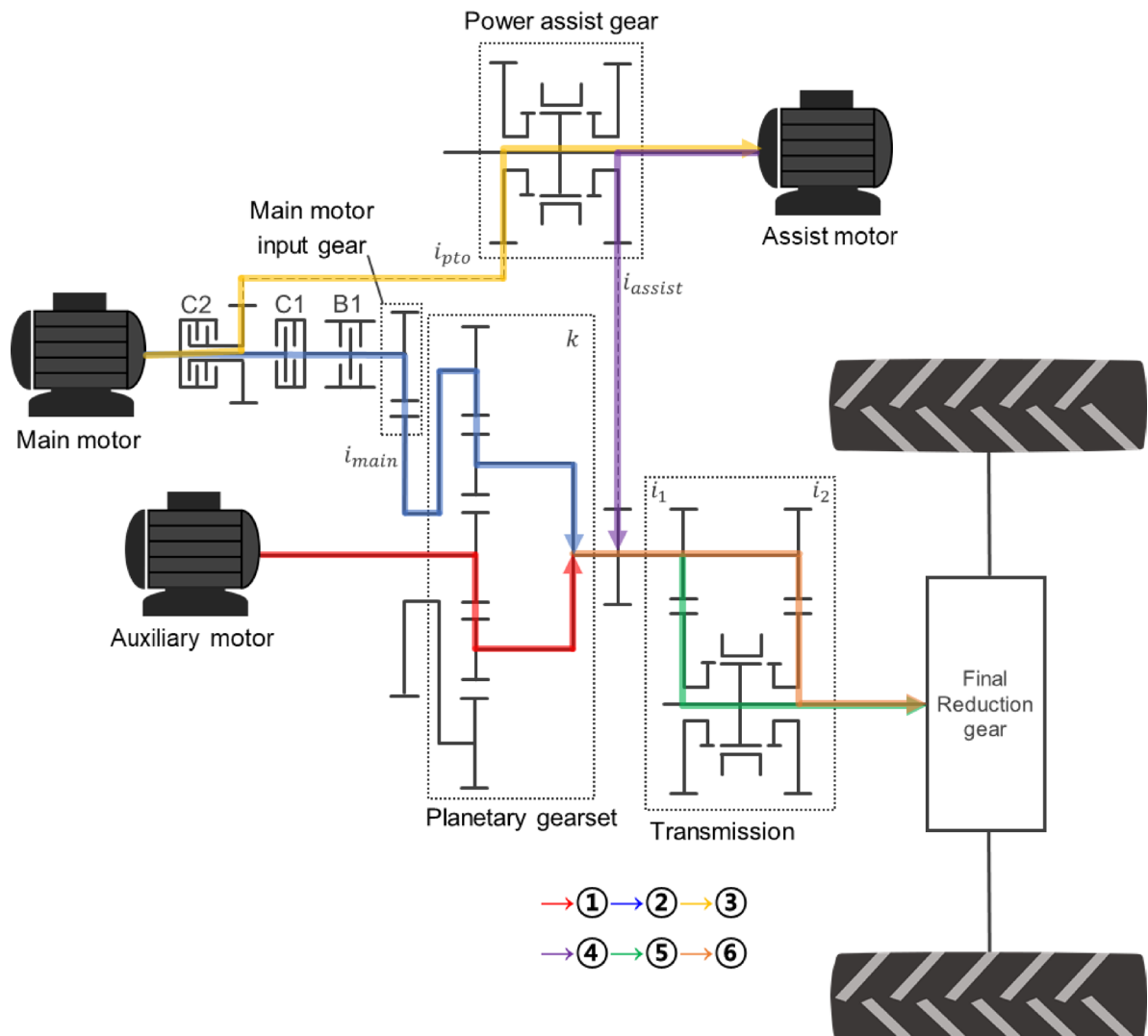


Fig. 4. DMCP with power assist system: mixed-coupling type.

In the assist mode, all three motors — the main motor, auxiliary motor, and assist motor — are engaged to provide maximum torque. The transmission gear is selected based on the operational requirements: the first gear is employed for low-speed, high-torque tasks, whereas the second gear is used for high-speed, moderate-torque conditions. In this mode, the torques of the three motors were combined as follows: When clutch C1 is engaged and both C2 and B1 are disengaged, the main motor drives the ring gear of the planetary gearset, and the auxiliary motor delivers torque to the sun gear. Concurrently, the assist motor directly contributes additional torque to the carrier via the power-assist gear through the auxiliary motor input gearset, which has a gear ratio i_{assist} . The total combined torque from the carrier was transmitted through the transmission to drive the wheels. The power flow paths for each gear stage, as illustrated in Fig. 4, are as follows: In the first gear, the main motor used paths 2 and 5, the auxiliary motor used paths 1 and 5, and the assist motor followed paths 4 and 5. In the second gear, the power from the main motor is transmitted along Paths 2 and 6, that from the auxiliary motor is transmitted along Paths 1 and 6, and that from the assist motor is transmitted along Paths 4 and 6.

3) PTO mode

The PTO mode functions similarly to the baseline DMCP and is activated when the power-assist system is disengaged. In this mode, the main motor transmits power to the PTO through the power-assist gear (gear ratio: i_{pto}) when clutch C1 is disengaged and C2 and B1 are engaged. Simultaneously, the auxiliary motor delivered torque to the drive wheels for traction. As shown in Fig. 4, the power from the main motor flows in the reverse direction of line 3, whereas the power from the auxiliary motor is routed along lines 1 and 5.

Table 3 details the engagement state of each powertrain component for the various operating modes.

Operating mode	Mainmotor	Auxiliary motor	Assistmotor	Clutch		Brake	TransmissionRatio	
				C1	C2		1st gear	2nd gear
Dual mode 1	●	●	○	●	○	○	●	○
Dual mode 2	●	●	○	●	○	○	○	●
Assist mode 1	●	●	●	●	○	○	●	○
Assist mode 2	●	●	●	●	○	○	○	●
PTO mode	●	●	○	○	●	●	●	○

Table 3. Operating modes of the DMCP power assist system: mixed-coupling type. • indicates that the motor is on or the brake is engaged, ○ indicates that the motor is off or the brake is disengaged

Components	Parameter	Value
Main motor	Rated speed, rpm	4000
	Maximum speed, rpm	6000
	Maximum torque, N·m	72 @ 4000 rpm
	Rated power, kW	30
Auxiliary motor/Assist motor	Rated speed, rpm	4000
	Maximum speed, rpm	6000
	Maximum torque, N·m	24 @ 4000 rpm
	Rated power, kW	10

Table 4. Parameters of motors.

Dynamic model of powertrains

A dynamic model of the tractor and its primary components was developed to analyze the performance of the three proposed powertrain configurations. For a fair comparison, identical specifications for the tractor and electric motors were applied across all configurations, with the only distinction being the powertrain configuration. Furthermore, several simplifying assumptions were made: (1) terrain-related effects were excluded by assuming zero tire slip and a level road surface; and (2) only the rotational inertias of the motors and wheels were considered. The longitudinal dynamics of the tractor are formulated as follows.

$$\sum I_w \dot{\omega}_{rw} = T_t - \sum T_{load} \quad (1)$$

$$\sum T_{load} = \left(fG + \frac{1}{2} \rho C_d A v^2 \right) r_{rw} \quad (2)$$

$$v = r_{rw} \omega_{rw} \quad (3)$$

Where, $\sum I_w$ is the moment of inertia of the tractor, $\dot{\omega}_{rw}$ is the acceleration of the rear wheel, T_t is the traction torque of the tractor, f is the rolling resistance coefficient of the tractor, G is the total gravity of the tractor, ρ is the air density, C_d is the air resistance coefficient, A is the windward area, v is the travel speed of the tractor, δ is the mass conversion coefficient, m is the mass of the tractor, r_{rw} is the radius of the rear wheel, ω_{rw} is the rotational speed of rear wheel and $\sum T_{load}$ is the load torque of the tractor.

Each electric motor is represented by a quasistatic model based on an interpolated efficiency map¹⁸. An identical motor model was applied to all configurations to isolate the performance effects of the powertrain configuration. The motor specifications summarized in Table 4 are based on a custom-developed motor for agricultural tractor applications. The efficiency map is presented in Fig. 5.

Speed-coupling type of DMCP

The dynamic model of the speed-coupling-type DMCP is based on a configuration in which the main motor is connected to the ring gear, the auxiliary motor is connected to the sun gear, and the carrier serves as the output. Based on the kinematics of the planetary gear set described in Eqs. (4) and (5), the motor torques are transmitted to the carrier at a constant ratio and the carrier speed is determined by the sum of the rotational speeds of the ring and sun gears.

$$\frac{k+1}{k} T_{ring} = (k+1) T_{sun} = T_{carrier} \quad (4)$$

$$\frac{k}{k+1} \omega_{ring} + \frac{1}{k+1} \omega_{sun} = \omega_{carrier} \quad (5)$$

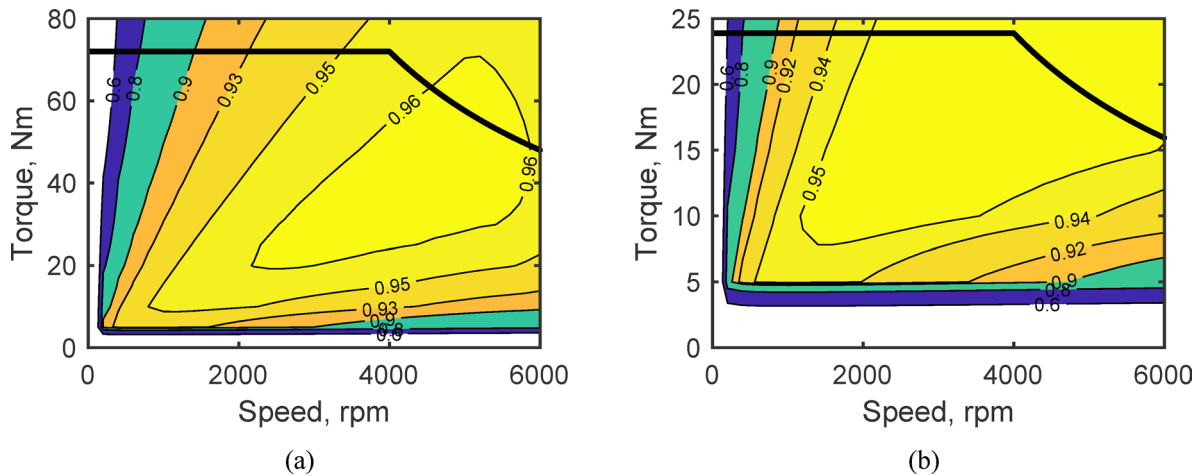


Fig. 5. Efficiency map of motors: **(a)** main motor; **(b)** auxiliary motor/assist motor.

Where, k is characteristics parameters of planetary gearset, T_{ring} is the torque of ring gear, T_{sun} is the torque of sun gear, $T_{carrier}$ is the torque of the planet carrier, ω_{ring} is the rotational speed of ring gear, ω_{sun} is the rotational speed of sun gear and $\omega_{carrier}$ is the rotational speed of the planet carrier.

Considering the kinematics of the planetary gear set, the dynamic model is expressed for each operating mode as follows:

1) Dual mode

$$(T_{main} - I_{main}\dot{\omega}_{main})i_{main} = T_{ring} \quad (6)$$

$$(T_{aux} - I_{aux}\dot{\omega}_{aux})i_{aux} = T_{sun} \quad (7)$$

$$T_{carrier} = \min \left(\frac{k+1}{k} T_{ring}, (k+1) T_{sun} \right) \quad (8)$$

$$T_{out} = T_{carrier} \quad (9)$$

$$T_{out}i_0i_j = T_t \quad (10)$$

Where, I_{main} is the moment of inertia of the main motor, $\dot{\omega}_{main}$ is the acceleration of the main motor, i_{main} is main motor input gear ratio, I_{aux} is the moment of inertia of the auxiliary motor, $\dot{\omega}_{aux}$ is the acceleration of auxiliary motor, i_{aux} is auxiliary motor input gear ratio, T_{out} is the transmission input torque, i_0 is the final reduction gear ratio and i_j is the transmission ratio ($j=1$ in first gear, $j=2$ in second gear).

2) PTO mode

$$\sum I_w\dot{\omega}_{rw} + I_{aux}\dot{\omega}_{aux}i_{aux}i_0i_j = T_{aux}i_{aux}i_0i_j - \sum T_{load} \quad (11)$$

$$\omega_{rw} = \frac{\omega_{aux}}{i_0i_j} \quad (12)$$

$$T_{out}i_0i_j = T_t \quad (13)$$

where i_{pto} is the PTO reduction ratio and $T_{pto_{load}}$ is the required torque at the PTO.

Speed-coupling type of DMCP with a power assist system

In the speed-coupling powertrain configuration with a power-assist system, the main and assist motors jointly deliver torque to the ring gear. In contrast, the auxiliary motor provides torque to the sun gear. The dynamic behavior in both the dual-mode and PTO modes remained identical to that of the baseline DMCP, as described by Eqs. (6)–(13). The dynamic model for the assist mode is formulated as follows:

$$\sum I_w\dot{\omega}_{rw} + I_{aux}\dot{\omega}_{aux}i_{aux}i_0i_j = T_{aux}i_{aux}i_0i_j - \sum T_{load} \quad (14)$$

$$\omega_{assist} = \frac{i_{assist}}{i_{pto}}\omega_{main} \quad (15)$$

$$(T_{aux} - I_{aux}\dot{\omega}_{aux})i_{aux2} = T_{sun} \quad (16)$$

$$T_{carrier} = \min \left(\frac{k+1}{k} T_{ring}, (k+1) T_{sun} \right) \quad (17)$$

$$T_{out} = T_{carrier} \quad (18)$$

$$T_{out} i_0 i_j = T_t \quad (19)$$

Where, T_{assist} is the torque of assist motor, I_{assist} is the moment of inertia of assist motor, i_{assist} is the gear ratio of assist motor, $\dot{\omega}_{assist}$ is the acceleration of the assist motor, ω_{assist} is the rotational speed of the assist motor, and i_{aux2} is auxiliary motor input gear ratio for assist mode.

The primary difference between the assist and dual modes is that the torque at the ring gear (T_{ring}) is determined by the sum of the torques from the main and assist motors (see Eq. (14)). According to planetary gear kinematics, the resulting carrier torque ($T_{carrier}$) is limited by the lower torque contributions from the ring (T_{ring}) and sun gears (T_{sun}) (see Eq. (17)). Therefore, to maximize the output torque ($T_{carrier}$), the sun gear torque (T_{sun}) must be increased. This is achieved in the assist mode by applying a dedicated gear reduction (i_{aux2}) to the input path of the auxiliary motor, thereby enabling a higher torque contribution from this motor compared to the dual mode.

Mixed-coupling type of DMCP with power assist system

In the mixed-coupling powertrain configuration with a power-assist system, the main and auxiliary motors were coupled to the planetary gear of the gearset and the sun gear, respectively. However, the assist motor is mechanically coupled directly to the carrier, that is, the transmission input shaft, via a power-assist gear. This arrangement allows the assist motor to contribute torque directly to the output, independent of the internal kinematics of the planetary gearset. Consequently, the dynamic models for the dual mode and PTO modes are identical to those of the baseline DMCP (Eqs. (6)–(13)). However, the dynamic model for the assist mode was extended as follows:

$$(T_{main} - I_{aux} \dot{\omega}_{main}) i_{main} = T_{ring} \quad (20)$$

$$T_{aux} - I_{aux} \dot{\omega}_{aux} = T_{sun} \quad (21)$$

$$T_{carrier} = \min \left(\frac{k+1}{k} T_{ring}, (k+1) T_{sun} \right) \quad (22)$$

$$T_{out} = T_{carrier} + (T_{assist} - I_{assist} \dot{\omega}_{assist}) i_{assist} \quad (23)$$

$$T_{out} i_0 i_j = T_t \quad (24)$$

$$\omega_{assist} = \frac{\omega_{carrier}}{i_{assist}} \quad (25)$$

Control strategy

For the dual-motor powertrain configurations evaluated in this study, the optimal power control strategy was inherently dependent on the specific power coupling method. Therefore, to ensure an objective comparison of the configurations, this study employed Dynamic Programming (DP). As a global optimization algorithm, DP determines the maximum achievable performance for each configuration, eliminating biases that would arise from using different predefined control strategies¹⁸.

The DP is a recursive optimization algorithm that determines a globally optimal control sequence by minimizing the cost function over a defined horizon¹⁹. In this study, a dynamic programming algorithm was used to identify the trajectory with the lowest energy consumption for each powertrain configuration while performing various agricultural tasks. Instead of relying on heuristic rule-based strategies, dynamic programming ensures optimality by evaluating all feasible control inputs at each time step. It then propagates the minimum cumulative cost-to-go via backward recursion, resulting in a globally optimal sequence of control inputs that minimizes total energy consumption based on the predicted load and velocity profiles.

In this study, the performance of each powertrain configuration was evaluated under plow tillage conditions by determining a control strategy that minimizes the required power. The load cycle was discretized into N time steps, where each step k was characterized by a state variable $x(k)$ and a control variable $u(k)$. Following the principle of optimality, the objective function determines the optimal control by minimizing the sum of the stage cost (denoted as $L(x(k), u(k))$) at step k and the optimal cost function from the subsequent step (denoted as $J^*(x(k+1))$), as shown in Eq. (28). The stage cost function is defined as the motor power required in that step. Given that plow tillage is a low-speed, high-torque task, the analysis was constrained to the first gear in both dual and assist modes. Table 5 summarizes the operating modes and the corresponding constraints applied in the dynamic programming, where modes 1 and 2 represent the dual and assist modes, respectively.

Because of the low travel speeds and high tractive loads inherent in agricultural operations, the potential for energy recovery through regenerative braking is negligible. Therefore, regenerative braking is excluded from the analysis²⁰. However, to prevent unrealistic behavior during the optimization process, such as excessive fluctuations in the motor speed and torque, two penalty terms were introduced to the cost function. These terms are used to calculate the virtual energy consumption, which more accurately reflects physical constraints^{18,21}. The first penalty term, the coefficient k_p , is designed to limit abrupt changes in the motor speed. As defined in Eq. (30), this penalty is calculated from the sum of the absolute changes in rotational speed ($\Delta \omega$) for each motor between a given time step t and the next, $t+1$. For this study, the variation limit (d_ω) was set to 3,000

Powertrain configurations	Working operation	
	Mode	Motors
Speed-coupling type of DCMP	$mode \in [1]$	$\omega_{main_min,k} \leq \omega_{main,k} \leq \omega_{main_max,k}$ $T_{main_min,k} \leq T_{main,k} \leq T_{main_max,k}$ $\omega_{aux_min,k} \leq \omega_{aux,k} \leq \omega_{aux_max,k}$ $T_{aux_min,k} \leq T_{aux,k} \leq T_{aux_max,k}$
Speed-coupling type of DCMP with power assist system Mixed-coupling type of DCMP with power assist system	$mode \in [1,2]$	$\omega_{main_min,k} \leq \omega_{main,k} \leq \omega_{main_max,k}$ $T_{main_min,k} \leq T_{main,k} \leq T_{main_max,k}$ $\omega_{aux_min,k} \leq \omega_{aux,k} \leq \omega_{aux_max,k}$ $T_{aux_min,k} \leq T_{aux,k} \leq T_{aux_max,k}$ $\omega_{assist_min,k} \leq \omega_{assist,k} \leq \omega_{assist_max,k}$ $T_{assist_min,k} \leq T_{assist,k} \leq T_{assist_max,k}$

Table 5. Constrains under working operation.

rpm/s over a 1-second time step. The second penalty term, a coefficient $\gamma \theta (k)$, is applied to suppress frequent mode switching by adding a virtual energy cost for each transition. While mode shifting incurs energy losses from actuating components, such as clutches and brakes, these were not explicitly modeled. Instead, the virtual penalty serves to curtail the unrealistic switching behavior that might arise from marginal efficiency advantages. The optimization effectively avoids non-physical motor behavior by incorporating these two penalty terms. The complete cost function is formulated as shown in Eqs. (32) and (33), and the actual energy consumption, which excludes the penalty terms, was calculated using Eq. (34).

$$x(k+1) = f(x(k), u(k)) \quad (26)$$

$$J^*_{N}(x(N)) = 0 \quad (27)$$

$$J^*(x(k)) = \min_{u(k)} [L(x(k), u(k)) + J^*(x(k+1))] \quad (28)$$

$$P_{req}(k) = P_{main}(k) + P_{aux}(k) + P_{assist}(k) = \frac{T_{main}\omega_{aux}}{\eta_{main}} + \frac{T_{aux}\omega_{aux}}{\eta_{aux}} + \frac{T_{assist}\omega_{assist}}{\eta_{assist}} \quad (29)$$

$$k_p = \begin{cases} 1 - \alpha \frac{\Delta\omega}{d_\omega \Delta t}, & \Delta\omega \leq d_\omega \Delta t \\ 0, & \Delta\omega \geq d_\omega \Delta t \end{cases} \quad (30)$$

$$\Delta\omega = |\omega_{main}(t_k+1) - \omega_{main}(t_k)| + |\omega_{aux}(t_k+1) - \omega_{aux}(t_k)| + |\omega_{assist}(t_{k+1}) - \omega_{assist}(t_k)| \quad (31)$$

$$\hat{P}_{req}(k) = k_p^{-sign(P_{req})} P_{req} + \gamma\theta(k) \quad (32)$$

$$L_{(X(k), u(k))} = \hat{P}_{req}(k) \quad (33)$$

$$J = \sum_{k=0}^N P_{req}(k) \quad (34)$$

Where, $x(k)$ is the state variable, $J^*_{N}(x(k))$ is the optimal cost function with penalty term of k^{th} step, $L(x(k), u(k))$ is the cost function with a penalty term of k^{th} step, k_p is the penalty coefficient of motor speed, α is the small coefficient for penalty coefficient, $\Delta\omega$ is the changing amount of motor speed, d_ω is the maximum changing rate of motor speed, Δt is the time step, $\hat{P}_{req}(k)$ is the energy consumption of motors with penalty, $\gamma\theta(k)$ is the mode switching penalty term, and J is the total cost function.

Power assist system performance analysis

Load data acquisition

To evaluate the performance of each powertrain configuration, an analysis was conducted using experimental data from the plow tillage operations. The experiments were performed under two representative workload conditions, using 46 kW and 55 kW tractors, respectively. The 46 kW tractor was equipped with a four-cylinder diesel engine delivering a maximum torque of 262 N·m at 1800 rpm and a rated power of 46 kW at 2300 rpm. The 55 kW tractor utilized a 55.4 kW engine with a maximum torque of 280 N·m at 1600 rpm.

Detailed specifications of the tractors and implements are summarized in Tables 6 and 7, respectively. During the field tests, each tractor was equipped with a six-row moldboard plow; the 46 kW tractor used the implement denoted as moldboard plow A in Table 7, whereas the 55 kW tractor used moldboard plow B. For the 55 kW tractor, a slightly wider variant (2100 mm overall width) was used, while all other geometric parameters were identical between A and B. The maximum tillage depth in both plots was 200 mm. Figure 6 depicts the experimental tractors and the test field during plow tillage.

To acquire agricultural workload data, real-time measurements of wheel torque and speed were collected. This was accomplished using torque meters mounted on all four wheels and gear tooth speed sensors (CYGTS21B; ChenYang Technologies GmbH & Co. KG, Germany). To eliminate the influence of terrain variability, the slip between the wheels and the ground was not considered. From these measurements, the key performance

Item	Specification		
	Tractor #1	Tractor #2	
Dimension	Length (mm)	3,695	3920
	Width (mm)	1,850	1940
	Height (mm)	2,560	2710
	Weight (kg)	2,615	2865
	Wheelbase (mm)	2,155	2190
	Minimum ground clearance (mm)	420	440
Transmission	Main part	Stages	4 stages
	Subpart	Stages	3 stages
	Type	Power shuttle	
Weight distribution	Front (%)	45.9	42.4
	Rear (%)	54.1	57.6
Tire	Front	11.2–20 8PR	11.2–24
	Rear	14.9–30 8PR	16.9–30
Engine	Type	4 cylinder diesel	4 cylinder diesel
	Rated power (kW)	46 @ 2,300 rpm	55.4 @ 2,200 rpm
	Max torque (N·m)	262 @ 1,800 rpm	280 @ 1,60 rpm

Table 6. Specifications of the agricultural tractors used in this study.

Item		Specification	
Type		Moldboard plow A	Moldboard plow B
Number of furrows	3	3	
Dimension	Length (mm)	1,930	1,930
	Width (mm)	1,800	2,100
	Height (mm)	1,235	1,235
Required power (kW)	40–52	52–60	
Weight (kg)	370	380	
Maximum tillage depth (mm)	200	200	

Table 7. Specifications of plows used in this study.

metrics, tractive force, and travel speed were determined. The total tractor-traction force (F_t) was calculated by first determining the force at each wheel from the measured torque (Eq. (35)) and summing these individual forces (see Eq. (36)). The tractor travel speed was derived from the measured wheel speed (see Eq. (37)).

$$F_w = \frac{T_w}{r_w} \quad (35)$$

$$F_w = \frac{T_w}{r_w} \quad (36)$$

$$v = \frac{2\pi\omega_w r_w}{60} \quad (37)$$

Where, F_w is wheel traction force, T_w is wheel torque, r_w is wheel radius, F_t is tractor total traction force, F_{frw} is traction force of the front right wheel, F_{flw} is traction force of the front left wheel, F_{rrw} is traction force of the rear right wheel, F_{rlw} is traction force of the rear left wheel and ω_w is wheel speed.

Plow tillage operations were conducted while maintaining a constant tillage depth. The 46 kW and 55 kW tractors were operated in M2 and M1 gears with target travel speeds of 4.6 km/h and 3.8 km/h, respectively. The resulting workload profile for the 46 kW tractor is presented in Fig. 7, and the profile for the 55 kW tractor is shown in Fig. 8. During the 46 kW tractor plowing test, the travel speed ranged from 2.62 to 4.56 km/h, with a mean of 3.90 km/h. The observed speed reductions were attributed to plow load and slip. The traction force reached a maximum of 23.60 kN and a mean of 9.69 kN. For the 55 kW tractor, the travel speed ranged from 3.26 to 3.80 km/h, with a mean of 3.89 km/h. The traction force exhibited a maximum of 27.92 kN and a mean of 19.93 kN. In both cases, the maximum traction force was observed as the tractor accelerated from a standstill toward the target speed.



(a)



(b)



(c)



(d)

Fig. 6. Experimental tractors and test field during plow tillage: (a) 46 kW tractor; (b) 55 kW tractor; (c) test field for 46 kW tractor; (d) test field for 55 kW tractor.

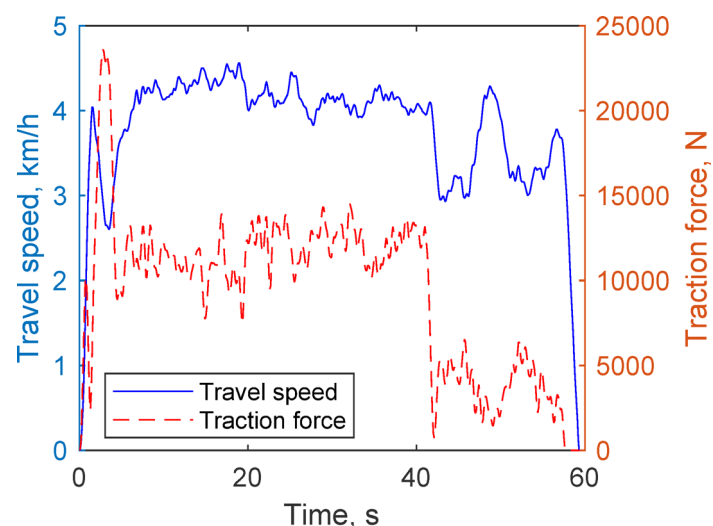


Fig. 7. Workload data during plow tillage with a 46 kW tractor: travel speed and traction force.

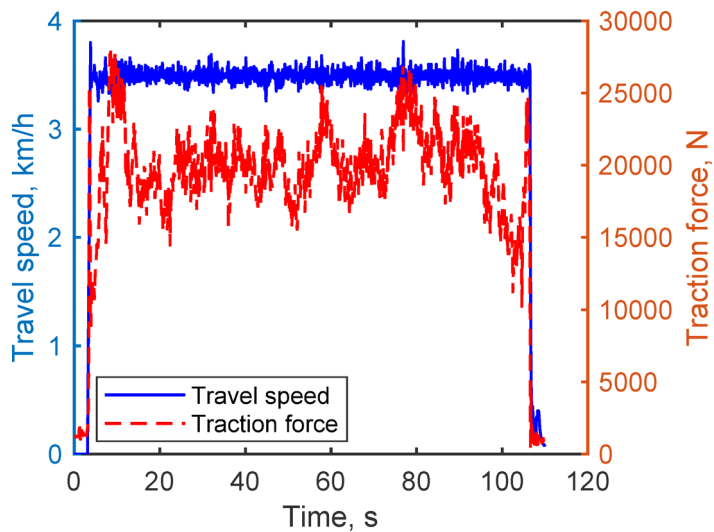


Fig. 8. Workload data during plow tillage with a 55 kW tractor: travel speed and traction force.

Agricultural work performance analysis

The objective of this study was to analyze agricultural work performance based on two primary factors: the application of a power-assist system and the structural differences between powertrain configurations. The performance evaluation is conducted using the previously acquired plowing load data and is divided into a dynamic performance analysis, which evaluates the operational capability, and an economic performance analysis, which evaluates the energy consumption.

In the dynamic performance analysis, the achievable travel speed and maximum tractive force for each powertrain configuration were calculated to assess the operational capability relative to the measured agricultural workload. To this end, the evaluation verified whether the operating points of the measured workload fell within the powertrain power envelope (F–V curve). This envelope, which consists of a constant traction force region and constant traction power region, is calculated using Eqs. (38)–(42).

$$F_t(V) = \int_0^{V_{t_{\max}}} F_{t_{\max}} + \int_{V_{t_{\max}}}^{V_{t_{\max}}} \frac{P_{t_{\max}}}{V} \quad (38)$$

$$T_{carrier_{\max}} = \min\left(\frac{k+1}{k} T_{ring_{\max}}, (k+1) T_{sun_{\max}}\right) \quad (39)$$

Transmission input torque:

- (1) Speed-coupling type of DMCP and speed-coupling type of DMCP with power assist system

$$T_{out} = T_{carrier_{\max}} \quad (40)$$

- (2) Mixed-coupling type of DMCP with power assist system

$$T_{out} = T_{carrier_{\max}} + T_{assist_{\max}} i_{assist} \quad (41)$$

$$F_{t_{\max}} = \frac{T_{out} i_0 i_1}{r_{rw}} \quad (42)$$

$$P_{t_{\max}} = V_{t_{\max}} F_{t_{\max}} \quad (43)$$

where $F_t(V)$ is the power envelope of the powertrain configuration, $V_{t_{\max}}$ is the maximum travel speed at the maximum traction force, V_{max} is the maximum travel speed of the tractor, and $P_{t_{\max}}$ is the maximum power of the tractor.

For economic performance analysis, a dynamic programming simulation was conducted for each powertrain configuration using the acquired workload data. The energy consumption of each configuration was compared under identical load conditions by applying the control strategy. The parameters used in the simulations are listed in Table 8. The auxiliary-motor input gear ratio and the assist gear ratio were determined as follows: Parameterization of the power-assist drivetrain. In the speed-coupling configuration, the auxiliary-motor input gear engages i_{aux1} in dual mode and i_{aux2} in assist mode. For dual mode, i_{aux1} is identical to the baseline auxiliary input ratio i_{aux} used in the speed-coupling DMCP; in assist mode, i_{aux2} is set to 1.4187, following planetary kinematics, to increase the effective sun-side torque and thereby maximize the torque transmitted

Parameter	Symbol	DMCP	DMCP with power assist system	
		Speed-coupling type	Speed-coupling type	Mixed-coupling type
Transmission gear ratio	i_1	4.03		
	i_2	1.963		
Final reduction gear ratio	i_0	37.4414		
PGS gear ratio	k	3.256		
Main motor input gear ratio	i_{main}	1		
Auxiliary motor input gear ratio	i_{aux}	1	-	-
	i_{aux1}	-	1	-
	i_{aux2}	-	1.4187	-
PTO gear ratio	i_{pto}	4.44		
Assist gear ratio	i_{assist}	-	0.2252	1
Rear wheel radius, m	r_r	0.594		
Moment of inertia of main motor, kg·m ²	I_{main}	0.04		
Moment of inertia of auxiliary motor, kg·m ²	I_{aux}	0.0066		
Moment of inertia of assist motor, kg·m ²	I_{assist}	0.0066		
The rolling resistance coefficient of tractor	f	0.05		
The total gravity of the tractor, N	G	40,967		
The air density, kg/m ³	ρ	1.225		
The air resistance coefficient	C_d	1		
The windward area, m ²	A	4.71		
Battery capacity Ah	Q	115.2		

Table 8. Main parameters of the tractor.

to the ring. The assist gear ratio (i_{assist}) is chosen as the reciprocal of the PTO ratio, 0.2252, so that the assist motor can continuously deliver torque up to the maximum shaft-speed region while its power is merged with that of the main motor. In the mixed-coupling configuration, the assist gear ratio is set to 1.0 to enable torque delivery up to the carrier's maximum shaft-speed region.

Results and discussion

Dynamic performance analysis

Figure 9 illustrates the workload operating points for each powertrain configuration plotted against their respective power envelopes (F-V curves). Under the 46 kW workload, all three configurations operated within their power envelopes, confirming their capability to perform the required plow tillage task. In contrast, under the more demanding 55 kW workload, only the configurations equipped with a power-assist system remained within the feasible power domain. The baseline DMCP configuration failed to provide sufficient tractive effort, particularly during peak load conditions, which impeded stable operation. A comparison of the maximum tractive forces revealed a clear hierarchy among the configurations. The baseline DMCP achieved the lowest value at 24.36 kN, whereas both power-assisted configurations yielded significantly higher forces. Specifically, the speed-coupling configuration reached 31.87 kN, and the mixed-coupling configuration reached 30.43 kN, with the speed-coupling configuration outperforming the mixed-coupling configuration. This difference is attributed to the torque contribution point of the assist motor, which determines the resulting maximum traction torque, even when the other powertrain parameters are identical. Table 9 summarizes the maximum tractive force and corresponding travel speed at that torque for each powertrain configuration. In the mixed-coupling configuration, the torque of the assist motor is directly applied to the transmission input shaft (i.e., the carrier of the planetary gearset). By contrast, the speed-coupling configuration delivers the torque of the assist motor to the ring gear. Owing to the planetary gear kinematics, this latter arrangement introduces a torque multiplication effect by a factor of $\frac{k+1}{k}$, resulting in a higher maximum traction torque compared with the mixed-coupling type. However, this torque amplification results in a tradeoff. In the assist mode of a speed-coupling configuration, the ring gear torque is the sum of the main and assist motor torques. Consequently, the torque of the sun gear must be increased proportionally to satisfy the kinematic constraints of the planetary gear. As the torque required from the sun gear (driven by the auxiliary motor) increases, the maximum allowable rotational speed decreases. This results in the speed-coupling configuration having a lower maximum travel speed in assist mode than in the mixed-coupling configuration.

Economic performance analysis

For the economic performance evaluation, two distinct plow tillage load conditions were considered, corresponding to 46 kW and 55 kW tractors. Under the 46 kW condition, the energy consumption of three powertrain configurations was compared: the baseline DMCP, speed-coupling DMCP with a power-assist

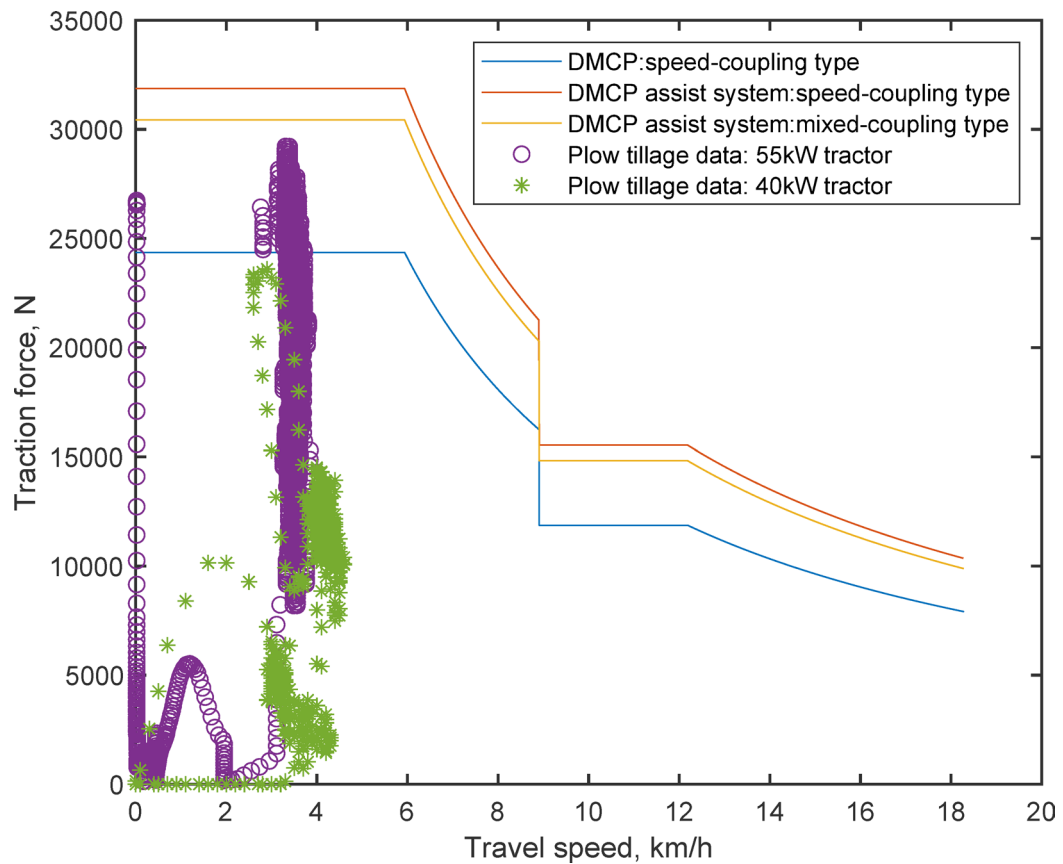


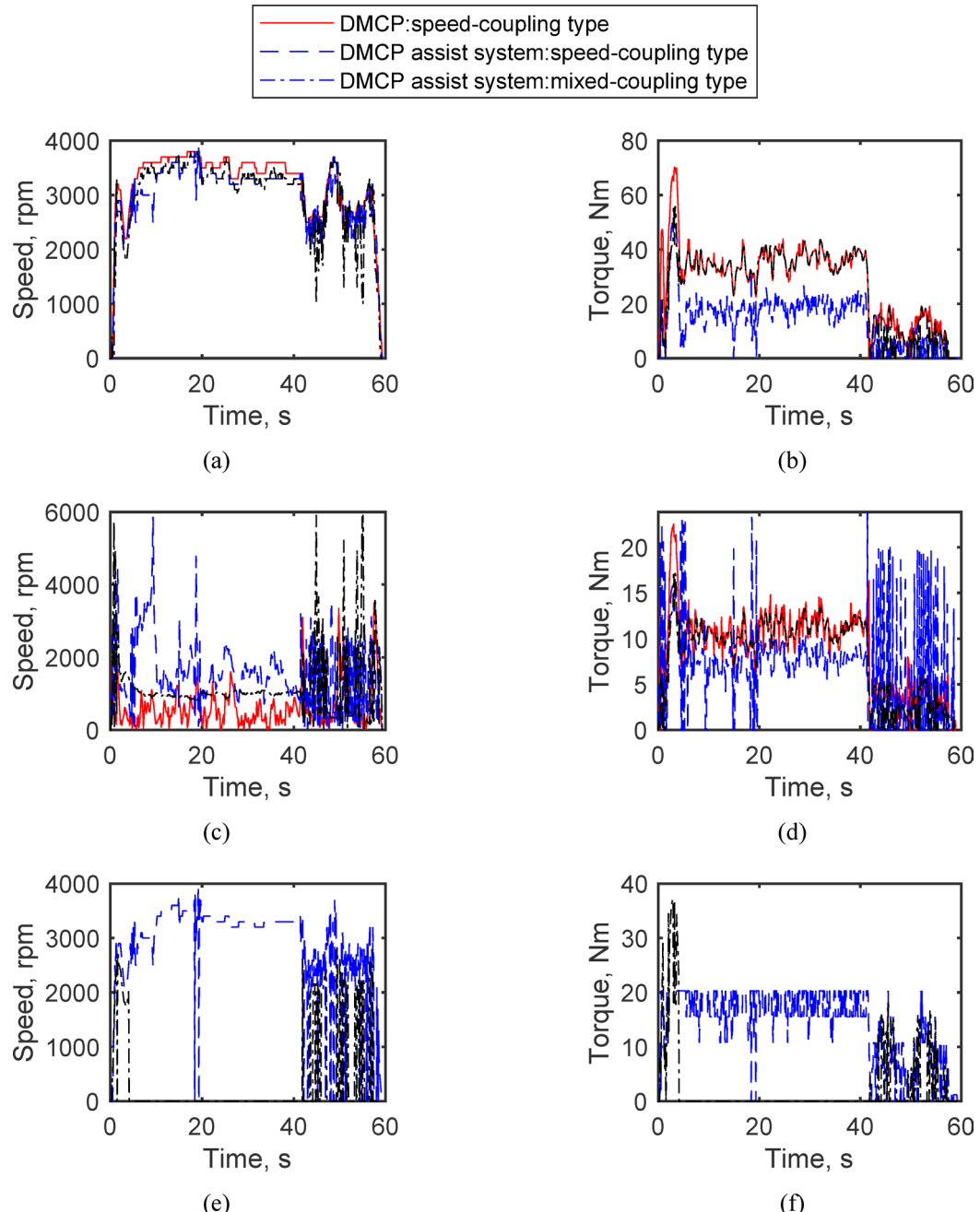
Fig. 9. Working points of different powertrain configurations under plow tillage operations.

Powertrain configurations	Dynamic performance	
	Maximum traction torque	Maximum travel speed at maximum traction torque
Speed-coupling type of DMCP	$\frac{k+1}{k} T_{main} i_0 i_1$	$\frac{1}{i_0 i_1} \frac{2\pi r_w}{60} \left(\frac{k}{k+1} \omega_{main} + \frac{1}{k+1} \omega_{aux} \right)$
Speed-coupling type of DMCP with power assist system	$\frac{k+1}{k} \left(T_{main} + \frac{i_{pto}}{i_{assist}} T_{assist} \right) i_0 i_1$	$\frac{1}{i_0 i_1} \frac{2\pi r_w}{60} \left(\frac{k}{k+1} \omega_{main} + \frac{1}{(k+1)i_{aux2}} \omega_{aux} \right)$
Mixed-coupling type of DMCP with power assist system	$\left(\frac{k+1}{k} T_{main} + T_{assist} i_{assist} \right) i_0 i_1$	$\frac{1}{i_0 i_1} \frac{2\pi r_w}{60} \left(\frac{k}{k+1} \omega_{main} + \frac{1}{k+1} \omega_{aux} \right)$

Table 9. Dynamic performance of powertrain configurations.

system, and mixed-coupling DMCP with a power-assist system. For the 55 kW condition, however, the comparison was limited to the two power-assist-equipped configurations because the baseline DMCP was unable to perform the task under this high workload. The energy consumption results summarized in Table 10 were calculated as the cumulative motor energy output (Eq. (34)) without accounting for the differences in mechanical efficiency arising from configuration variations. Under the 46 kW workload, the speed-coupling and mixed-coupling DMCP with power-assist systems achieved energy reductions of 2.40% and 1.78%, respectively, compared to the baseline DMCP. This improvement is attributed to the ability of the three-motor configuration to operate at more efficient points by flexibly distributing the required load across the motors. Under the 55 kW workload, the speed-coupling DMCP with a power-assist system consumed 0.41% less energy than its mixed-coupling counterpart. Figure 10 shows the motor operating points under the 46 kW workload, while the results for the 55 kW condition are provided in Supplementary Fig. S1. For the speed-coupling DMCP with a power-assist system, the main motor operates at a lower torque level than the baseline DMCP because the assist motor compensates for the required torque difference. This load redistribution enables motors to operate in more efficient regions, thereby enhancing the overall system efficiency. Furthermore, the power-assist gear introduces a higher effective gear ratio for the power path of the auxiliary motor, which reduces the torque required from the auxiliary motor compared to the baseline configuration. In the mixed-coupling configuration, the dual mode was primarily selected during the 10–40 s interval. This behavior is explained by the penalty-based constraints within the DP algorithm, which identify the dual mode as a more energy-efficient option during a specific

Powertrain	Energy consumption under plow tillage operation, kWh	
	46 kW workload	55 kW workload
Speed-coupling type of DMCP	0.1794	-
Speed-coupling type of DMCP with power assist system	0.1751	0.5778
Mixed-coupling type of DMCP with power assist system	0.1762	0.5802

Table 10. Energy consumption of powertrain configurations under different agricultural work conditions.**Fig. 10.** Motor operating curves of different powertrain configurations under plow tillage operation of 46 kW workload: **a** Main motor speed; **b** Main motor torque; **(c)** Auxiliary motor speed; **(d)** Auxiliary motor torque; **(e)** Assist motor speed; **(f)** Assist motor torque.

period. Outside this interval, the assist mode was predominantly used, resulting in the concurrent operation of all three motors and, consequently, a lower total energy consumption than the baseline DMCP. In summary, the powertrain configurations equipped with a power-assist system demonstrated superior energy efficiency compared with the baseline DMCP. This validates the proposed power-assist architecture as a viable solution for optimizing the energy consumption of agricultural tractors.

Conclusion

This study proposes a PTO-based power-assisted system for electric tractors to enhance their traction performance and high-load operability. Three powertrain configurations were comparatively analyzed: (1) a baseline DMCP, (2) a speed-coupling DMCP with a power-assist system, and (3) a mixed-coupling DMCP with a power-assist system.

The dynamic performance analysis showed that, while all configurations could perform the task under a 46 kW workload, only those equipped with a power-assist system operated within the feasible power envelope under the more demanding 55 kW workload. Notably, the speed-coupling configuration with the power-assisted system achieved the highest maximum traction torque, which was attributed to its torque amplification effect. However, its maximum travel speed was reduced owing to kinematic constraints.

In the economic performance analysis evaluated using Dynamic Programming, the power-assist-equipped configurations consumed up to 2.40% less energy than the baseline DMCP. The speed-coupling type demonstrated the highest efficiency, which was attributed to the ability of the three-motor system to distribute the required load flexibly and operate each motor closer to its optimal efficiency point.

In conclusion, the proposed PTO-based power-assist system offers a practical and scalable solution for improving both the tractive capability and energy efficiency of electric tractors without major structural modifications. These findings provide valuable design guidelines for future electric-tractor powertrains. Future work will focus on hardware-in-the-loop validation and the implementation of real-time control strategies to assess their practical feasibility.

Data availability

The datasets used and/or analyzed during the current study available from the corresponding author on reasonable request.

Received: 13 August 2025; Accepted: 3 December 2025

Published online: 10 December 2025

References

1. Moreda, G. P., Muñoz-García, M. A. & Barreiro, P. High voltage electrification of tractor and agricultural machinery - A review. *Energy Convers. Manag.* **115**, 117–131 (2016).
2. Li, T., Xie, B., Li, Z. & Li, J. Design and optimization of a dual-input coupling powertrain system: a case study for electric tractors. *Appl. Sci.* **10**, 1608 (2020).
3. Ueka, Y., Yamashita, J., Sato, K. & Doi, Y. Study on the development of the electric tractor: specifications and traveling and tilling performance of a prototype electric tractor. *Eng. Agric. Environ. Food* **6**, 160–164 (2013).
4. Li, X. et al. Parameters collaborative optimization design and innovation verification approach for fuel cell distributed drive electric tractor. *Energy* **292**, 130485 (2024).
5. Wang, S. et al. Co-optimization energy management strategy for a novel dual-motor drive system of electric tractor considering efficiency and stability. *Energy* <https://doi.org/10.1016/j.energy.2023.128074> (2023).
6. Melo, R. R. et al. Conception of an electric propulsion system for a 9 kW electric tractor suitable for family farming. *IET Electr. Power Appl.* **13**, 1993–2004 (2019).
7. Borhan, H. et al. Predictive hierarchical eco-driving control involving speed planning and energy management for connected plug-in hybrid electric vehicles. *Energy* **283**, 473–493 (2023).
8. Baek, S., Jeon, H., Kim, W., Kim, Y. & Kim, Y. Design and analysis of a power transmission system for 55 kW electric tractor using agricultural workload data. *Sci. Rep.* **15**, 28028 (2025).
9. Deng, X. et al. Research on dynamic analysis and experimental study of the distributed drive electric tractor. *Agriculture* **13**, 40 (2023).
10. Liu, M., Li, Y., Xu, L., Wang, Y. & Zhao, J. General modeling and energy management optimization for the fuel cell electric tractor with mechanical shunt type. *Comput. Electron. Agric.* **213**, 108178 (2023).
11. Liu, M. et al. Optimal design of an adaptive energy management strategy for a fuel cell tractor operating in ports. *Comput. Electron. Agric.* **11**, 118801–118811 (2023).
12. Li, X., Xu, L., Liu, M., Yan, X. & Zhang, M. Research on torque cooperative control of distributed drive system for fuel cell electric tractor. *Comput. Electron. Agric.* **219**, 108811 (2024).
13. Li, Y., Liu, M., Wang, Y., Xu, L. & Lei, S. Energy management optimization and validation of a hydrogen fuel Cell-Powered agricultural tractor based on hierarchical dynamic programming. *IEEE Access* **12**, 21382–21401 (2024).
14. Zhang, S. et al. A combined control method of traction and ballast for an electric tractor in ploughing based on load transfer. *Comput. Electron. Agric.* **207**, 107750 (2023).
15. Wen, C. et al. Design and verification innovative approach of dual-motor power coupling drive systems for electric tractors. *Energy* **247**, 123538 (2022).
16. Molaro, G. & Sedoni, E. Experimental evaluation of power losses in a power-shift agricultural tractor transmission. *Biosyst. Eng.* **100**, 177–183 (2008).
17. Wang, Z., Zhou, J. & Rizzoni, G. A review of architectures and control strategies of dual-motor coupling powertrain systems for battery electric vehicles. *Renew. Sustain. Energy Rev.* **162**, 112455 (2022).
18. Du, W., Zhao, S., Jin, L., Gao, J. & Zheng, Z. Optimization design and performance comparison of different powertrains of electric vehicles. *Mech. Mach. Theory* **156**, 104143 (2021).
19. Bellman, R. Dynamic programming. *Science* **153**, 34–37 (1966).
20. Barthel, J., Gorges, D., Bell, M. & Munch, P. Energy management for hybrid electric tractors combining load point shifting, regeneration and boost. in *IEEE Vehicle Power and Propulsion Conference (VPPC)* 1–6 (IEEE, 2014). 1–6 (IEEE, 2014). (2014).
21. Wu, J. & Zhang, N. Driving mode shift control for planetary gear based dual motor powertrain in electric vehicles. *Mech. Mach. Theory* <https://doi.org/10.1016/j.mechmachtheory.2020.104217> (2021).

Acknowledgements

This research was carried out with the assistance of the Korea Institute of Industrial Technology as “Development of smart electric driving platform by eco-friendly power source in agricultural work environment” (KITECH JA- 25-0008).

Author contributions

Conceptualization: A.D.V and W.G.K.; Methodology: A.D.V and W.G.K.; Code development: A.D.V and K.D.K.; Investigation: S.J.C and K.J.C.; Writing—original draft preparation: A.D.V.; Visualization: A.D.V and J.T.K.; Supervision: W.G.K. All authors have read and agreed to the published version of the manuscript.

Funding

This research was carried out with the assistance of the Korea Institute of Industrial Technology as “Development of smart electric driving platform by eco-friendly power source in agricultural work environment” (KITECH JA- 25 – 0008).

Declarations

Competing interests

The authors declare no competing interests.

Additional information

Supplementary Information The online version contains supplementary material available at <https://doi.org/10.1038/s41598-025-31465-5>.

Correspondence and requests for materials should be addressed to W.K.

Reprints and permissions information is available at www.nature.com/reprints.

Publisher's note Springer Nature remains neutral with regard to jurisdictional claims in published maps and institutional affiliations.

Open Access This article is licensed under a Creative Commons Attribution-NonCommercial-NoDerivatives 4.0 International License, which permits any non-commercial use, sharing, distribution and reproduction in any medium or format, as long as you give appropriate credit to the original author(s) and the source, provide a link to the Creative Commons licence, and indicate if you modified the licensed material. You do not have permission under this licence to share adapted material derived from this article or parts of it. The images or other third party material in this article are included in the article's Creative Commons licence, unless indicated otherwise in a credit line to the material. If material is not included in the article's Creative Commons licence and your intended use is not permitted by statutory regulation or exceeds the permitted use, you will need to obtain permission directly from the copyright holder. To view a copy of this licence, visit <http://creativecommons.org/licenses/by-nc-nd/4.0/>.

© The Author(s) 2025